The First Year Progress Report

on

WAVELET SPECTRAL FINITE ELEMENTS FOR WAVE PROPAGATION IN COMPOSITE PLATES WITH DAMAGES

Submitted to

Asian Office of Aerospace Research and Development (AOARD)
Tokyo, Japan
(Programme Manager: Dr. Kumar V Jata)

Principle Investigator:
Dr. S. Gopalakrishnan
Professor, Department of Aerospace Engineering,
Indian Institute of Science, Bangalore 560 012
India

March 24, 2010

Report Documentation Page

Form Approved
OMB No. 0704-0188

1. REPORT DATE	2. REPORT TYPE	3. DATES COVERED
24 MAR 2010	**Final**	**31-03-2009 to 30-03-2010**

4. TITLE AND SUBTITLE	5a. CONTRACT NUMBER
Wavelet spectral finite elements for wave propagation in composite plates with damages	**FA23860914022**
	5b. GRANT NUMBER
	5c. PROGRAM ELEMENT NUMBER
6. AUTHOR(S) **S. Gopalakrishnan**	5d. PROJECT NUMBER
	5e. TASK NUMBER
	5f. WORK UNIT NUMBER
7. PERFORMING ORGANIZATION NAME(S) AND ADDRESS(ES) **Indian Institute of Science,Indian Institute of Science,Bangalore,India,IN,560012**	8. PERFORMING ORGANIZATION REPORT NUMBER **N/A**
9. SPONSORING/MONITORING AGENCY NAME(S) AND ADDRESS(ES) **Asian Office of Aerospace Research & Development, (AOARD), Unit 45002, APO, AP, 96338-5002**	10. SPONSOR/MONITOR'S ACRONYM(S) **AOARD**
	11. SPONSOR/MONITOR'S REPORT NUMBER(S) **AOARD-094022**

12. DISTRIBUTION/AVAILABILITY STATEMENT
Approved for public release; distribution unlimited

13. SUPPLEMENTARY NOTES

14. ABSTRACT

For the Current Year (2009-2010), a new spectral plate element (SPE) for laminated composite using Daubechies compactly supported wavelet basis functions is developed to analyze wave propagation in an anisotropic laminated composite media. The element is based on the Classical Laminated Plate Theory (CLPT). The element is formulated using the recently developed methodology of spectral finite element formulation based on the solution of a Polynomial Eigenvalue Problem (PEP). By virtue of its frequency wavenumber domain formulation, single element is sufficient to model large structures where conventional finite element method will incur heavy cost of computation. First the Wavelet spectral element procedure is outlined, which is followed by a section on wavenumber computation as a function of fiber directions is given. A number of numerical examples are provided to show the efficiency of the formulated element. In most cases, the results from the wavelet formulations is compared with the conventional finite elements to show the computational superiority of the formulated wavelet spectral element for certain class of problems.

15. SUBJECT TERMS
Finite Element Methods, Wave propagation , Wave propagation , Structural Health Monitoring

16. SECURITY CLASSIFICATION OF:			17. LIMITATION OF ABSTRACT	18. NUMBER OF PAGES	19a. NAME OF RESPONSIBLE PERSON
a. REPORT **unclassified**	b. ABSTRACT **unclassified**	c. THIS PAGE **unclassified**	**Same as Report (SAR)**	**20**	

WAVELET SPECTRAL FINITE ELEMENTS FOR WAVE PROPAGATION IN COMPOSITE PLATES WITH DAMAGES

S. Gopalakrishnan, Indian Institute of Science, Bangalore, India

ABSTARCT

For the Current Year (2009-2010), A new spectral plate element (SPE) for laminated composite using Daubechies compactly supported wavelet basis functions is developed to analyze wave propagation in an anisotropic laminated composite media. The element is based on the Classical Laminated Plate Theory (CLPT). The element is formulated using the recently developed methodology of spectral finite element formulation based on the solution of a Polynomial Eigenvalue Problem (PEP). By virtue of its frequency-wavenumber domain formulation, single element is sufficient to model large structures, where conventional finite element method will incur heavy cost of computation. First the Wavelet spectral element procedure is outlined, which is followed by a section on wavenumber computation as a function of fiber directions is given. A number of numerical examples are provided to show the efficiency of the formulated element. In most cases, the results from the wavelet formulations is compared with the conventional finite elements to show the computational superiority of the formulated wavelet spectral element for certain class of problems.

1. INTRODUCTION

Composites are being used in aircraft structures because of their several favorable properties. Study of wave propagation in such composite structures is of much relevance because it helps one to understand their behavior under high-frequency impact load encountered in gust, bird hit, tool drop, etc. Apart from this, wave propagation analysis finds important applications in structural health monitoring using diagnostic waves, control of noise, and vibration. However, the behavior of composites at high frequencies is more complicated than it is for their metallic counterpart because of the presence of anisotropy, and very little literature is specifically available on transient wave propagation analysis of composite structures.

Wave propagation deals with loading of high-frequency content and FE formulation for such problems is computationally prohibitive because it requires large system size to capture all the higher modes. These problems are usually solved in the transformed frequency domain using Fourier Transform based methods and FFT Based Spectral Element formulation (FSFE) [1, 2] is one such method, especially tailored for wave propagation analysis. In FSFE formulation for 2D structures [1], nodal displacements are related to nodal tractions through a frequency-wave-number dependent stiffness matrix. The mass distribution is captured exactly, and the accurate elemental dynamic stiffness matrix is derived. Consequently, in the absence of any discontinuities, one element is sufficient to model a plate structure of any length, but unbounded along the other lateral direction.

The main drawback of FSFE is that it cannot handle waveguides of short lengths. This is because the required assumption of periodicity in time approximation results in a "*wraparound*" problem for a smaller time window, which totally distorts the response. However, in the proposed wavelet based Spectral element formulation (WSEM) , the use of Daubechies compactly supported wavelets [3] with localized basis for temporal approximation removes the signal wraparound problem and can efficiently model undamped finite length waveguides. In addition, for 2D problems, FSFEs [1] are essentially semi-infinite, *i.e*., they are bounded only in one direction. Thus, the effect of one lateral boundary cannot be captured, and this can be attributed to the global basis functions of the Fourier series approximation of the spatial dimension. The formulated 2D WSEM also overcomes the above problem and can accurately model 2D plate structures of finite dimensions. This is again due to the use of localized Daubechies scaling functions as the basis for approximation of the spatial dimension.

The steps followed in 2D WSFE formulation are as follows. Here, first Daubechies scaling functions are used for approximation in time and this reduces the governing partial differential equation (PDE) into a set of coupled PDEs in spatial dimensions. The wavelet extrapolation technique [4] is used for adapting wavelets in finite domain and imposition of initial conditions. The coupled transformed PDEs are decoupled through eigen analysis. This temporal approximation, imposition of initial conditions, and decoupling of the reduced PDEs are very similar to that done in WSEM formulation for 1D waveguides [5]. Next, each of these decoupled PDEs are further reduced to a set of coupled ODEs by using the same Daubechies scaling functions for approximation of the spatial dimension. Unlike the temporal approximation, here, the scaling function coefficients lying outside the finite domain are not extrapolated but obtained through periodic extension for unrestrained, *i.e.,* free lateral edges. Each set of ODEs are also coupled, and decoupling is again done using eigen value analysis.

Presence of elastic coupling in anisotropic laminated composite plate results in coupled governing differential equations. Thus, the final reduced ODEs after spatial and temporal approximations are in the form of a set of coupled ODEs, for each temporal and spatial sampling point. The solution of these ODEs to derive the exact shape function involves determination of wavenumbers and the amplitude ratio matrix. Unlike isotropic cases, here the process of solution is more complicated and is done by posing it as polynomial eigenvalue problem (PEP). It should be mentioned here that similar to 2D FSEM, the frequency-dependent wave characteristics corresponding to each lateral (Y) wavenumber, can be extracted directly from the present 2D WSEM formulation. However, unlike FSEM, the wavenumbers will be accurate only up to a certain fraction of Nyquist frequency [6].

2. Daubechies Compactly Supported Wavelets

In this section, a concise review of orthogonal basis of Daubechies wavelets [3] is provided. Wavelets $\psi_{j,k}(t)$ form a compactly supported orthonormal basis for $\mathbf{L}^2(\mathrm{R})$. The wavelets and associated scaling functions $\varphi_{j,k}(t)$ are obtained by translation and dilation of single functions $\psi(t)$ and $\varphi(t)$, respectively,

$$\psi_{j,k}(t) = 2^{j/2}\psi(2^j t - k), \quad j,\ k \in \mathbf{Z} \tag{1}$$

$$\varphi_{j,k}(t) = 2^{j/2}\varphi(2^j t - k), \quad j,\ k \in \mathbf{Z} \tag{2}$$

The scaling functions $\varphi(t)$, are derived from the dilation or scaling equation,

$$\varphi(t) = \sum_k a_k \varphi(2t - k) \tag{3}$$

and the wavelet function $\psi(t)$ is obtained as

$$\psi(t) = \sum_k (-1)^k a_{1-k} \varphi(2t - k) \tag{4}$$

where, a_k are the filter coefficients, which are fixed for a specific wavelet or scaling function basis. For compactly supported wavelets, only a finite number of a_k are nonzero. The filter coefficients a_k are derived by imposing certain constraints on the scaling functions.

Let $P_j(f)(t)$ be the approximation of a function $f(t)$ in $\mathbf{L}^2(\mathbf{R})$ using $\varphi_{j,k}(t)$ as the basis, at a certain level (resolution) j, then

$$P_j(f)(t) = \sum_k c_{j,k}\varphi_{j,k}(t), \quad k \in \mathbf{Z} \tag{5}$$

where $c_{j,k}$ are the approximation coefficients.

3. **Reduction of Wave Equations to ODEs**

3.1 Governing Differential Equations

Using classical laminated plate theory (CLPT) [8] the three governing equations with respect to the three degrees of freedom $u_o, v_o,$ and w are given below (Eqns(6-8)). Here, $u_0(x, y, t)$, $v_o(x, y, t)$, and $w(x, y, t)$ are the axial and transverse displacements in x, y and z directions, respectively, along the mid plane, which is at z = 0.

$$\frac{A_{11}\partial^2 u_0}{\partial x^2} + \frac{(A_{12} + A_{66})\partial^2 v_0}{\partial x\,\partial y} + \frac{A_{66}\partial^2 u_0}{\partial y^2} - \frac{B_{11}\partial^3 w}{\partial y^3} - \frac{(B_{12} + 2B_{66})\partial^3 w}{\partial x\,\partial y^2} = I_0 \ddot{u}_0 \tag{6}$$

$$\frac{A_{66}\partial^2 v_0}{\partial x^2} + \frac{(A_{12} + A_{66})\partial^2 u_0}{\partial x\,\partial y} + \frac{A_{22}\partial^2 v_0}{\partial y^2} - \frac{(B_{12} + 2B_{66})\,\partial w^3}{\partial x^2\,\partial y} - \frac{B_{22}\,\partial w^3}{\partial y^3} = I_0 \ddot{v}_0 \tag{7}$$

$$\frac{B_{11}\partial^3 u_0}{\partial x^3}+\frac{(B_{12}+2B_{66})\partial^3 u_0}{\partial x^2\,\partial y}+\frac{(B_{12}+2B_{66})\partial^3 v_0}{\partial x\,\partial y^2}+\frac{B_{11}\partial^3 v_0}{\partial x^3}$$
$$-\frac{D_{11}\partial^4 w}{\partial x^4}-\frac{2(D_{12}+2D_{66})\partial^4 w}{\partial x^2\,\partial y^2}-\frac{D_{22}\partial^4 w}{\partial y^4}$$
$$=I_0\ddot{w}-I_2\left(\frac{\partial^2\ddot{w}}{\partial x^2}+\frac{\partial^2\ddot{w}}{\partial y^2}\right) \qquad (8)$$

The stiffness coefficients A_{ij}, B_{ij}, D_{ij} and the inertial coefficients I_0, I_2 are defined as

$$[A_{ij},B_{ij},D_{ij}]=\int_A Q_{ij}[1,z,z^2]dA \quad [I_0,I_2]=\int_A \rho[1,z^2]dA$$

where Q_{ij} is the stiffness constant of the lamina and ρ is the mass density. The associated boundary conditions for edges parallel to Y-axis are

$$N_x=\frac{A_{11}\,\partial u_0}{\partial x}+\frac{A_{12}\,\partial v_0}{\partial y}-\frac{B_{11}\partial^2 w}{\partial x^2}-\frac{B_{12}\partial^2 w}{\partial y^2} \qquad (9)$$

$$N_y=A_{66}\left(\frac{\partial u_0}{\partial y}+\frac{\partial v_0}{\partial x}\right)-\frac{2B_{66}\partial^2 w}{\partial x\,\partial y} \qquad (10)$$

$$M_y=-\frac{B_{11}\,\partial u_0}{\partial x}-\frac{B_{12}\,\partial v_0}{\partial y}+\frac{D_{11}\partial^2 w}{\partial x^2}+\frac{D_{12}\partial^2 w}{\partial y^2} \qquad (11)$$

$$V=\frac{B_{11}\partial^2 u_0}{\partial x^2}+\frac{B_{12}\partial^2 v_0}{\partial x\,\partial y}-\frac{D_{11}\partial^3 w}{\partial x^3}-\frac{D_{12}\partial^3 w}{\partial x\,\partial y^2}+\frac{I_2\,\partial\ddot{w}}{\partial x} \qquad (12)$$

where N_x and N_y are the normal forces in x and y direction, respectively. M_y is the moments about y-axis. The shear resultant or the Kirchoff shear [1] V is obtained as

$$V=Q-\frac{\partial M_{xy}}{\partial y} \qquad (13)$$

where Q is the transverse shear force in the z direction. Next, governing PDEs and the associated boundary conditions derived here are reduced to a set of ODEs using Daubechies scaling function approximation in time and one spatial (Y) dimension.

3.2 Temporal Approximation.

The first step in the formulation of the 2D WSEM is the reduction of each of the three governing differential equations given by Eqs. (6–8) to a set of PDEs by Daubechies scaling function-based transformation in time. The procedure is exactly similar to that in the formulation of the 1D WSFE [5]. However, the key steps are stated here very briefly

for completeness. Let $u_0(x, y, t)$ be discretized at n points in the chosen time window$[0\, t_f]$ Let $\tau = 0,1, \ldots, n-1$ be the sampling points, then

$$t = \Delta t \tau \tag{14}$$

where Δt is the time interval between two sampling points. The function $u_0(x, y, t)$ can be approximated by scaling function $\varphi(\tau)$ at an arbitrary scale as

$$u_0(x,y,t) = u_0(x,y,\tau) = \sum_k u_{0k}(x,y)\varphi(\tau - k), \quad k \in \mathbf{Z} \tag{15}$$

where $u_{0k}(x, y)$ (referred as u_{0k} hereafter) are the approximation coefficients at a certain spatial dimension x and y. The other displacements $v_0(x, y, t)$, $w(x, y, t)$ can be transformed similarly. Substituting these approximations in Eqn. (6), using the orthogonality property of the translates of the scaling functions and the definition of connection coefficients [8], the transformed coupled PDEs obtained are of the form

$$A_{11}\left\{\frac{\partial^2 u_{0j}}{\partial x^2}\right\} + (A_{12} + A_{66})\left\{\frac{\partial^2 v_{0j}}{\partial x\, \partial y}\right\} + A_{66}\left\{\frac{\partial^2 u_{0j}}{\partial y^2}\right\} - B_{11}\left\{\frac{\partial^3 w_j}{\partial x^3}\right\}$$
$$- (B_{12} + 2B_{66})\left\{\frac{\partial^3 w_j}{\partial x\, \partial y^2}\right\} = [\Gamma^1]^2 I_0\{u_{0j}\} \tag{16}$$

where Γ^1 is the first-order connection coefficient matrix obtained after using the wavelet extrapolation technique [4]. These coupled PDEs are decoupled using eigenvalue analysis of Γ^1 as given in Reference [5]. The final decoupled form of the reduced PDEs given in Eqn (16) is

$$A_{11}\frac{\partial^2 \hat{u}_{0j}}{\partial x^2} + (A_{12} + A_{66})\frac{\partial^2 \hat{v}_{0j}}{\partial x\, \partial y} + A_{66}\frac{\partial^2 \hat{u}_{0j}}{\partial y^2} - B_{11}\frac{\partial^3 \hat{w}_j}{\partial x^3}$$
$$- (B_{12} + 2B_{66})\frac{\partial^3 \hat{w}_j}{\partial x\, \partial y^2} = -I_0 \gamma_j^2 \hat{u}_{0j} \quad j = 0, 1, \ldots, n-1 \tag{17}$$

where $\hat{u}_{oj}$ and similarly other transformed displacements are

$$\hat{u}_{0j} = \Phi^{-1} u_{0j} \tag{18}$$

where Φ is the eigenvector matrix of Γ^1 and γ_j are the corresponding eigenvalues. Following exactly similar steps, the two other governing differential equations (Eqs. (7) and (8)) and the force boundary conditions (Eqs.(9)–(12)) are transformed to PDEs in x and y.

It should be mentioned here that the sampling rate Δt should be less than a certain value to avoid spurious dispersion in the simulation using WSEM. In Reference [6], a numerical study has been presented from which the required Δt can be determined

depending on the order *N* of the Daubechies scaling function and frequency content of the load.

3.3 Spatial (*Y*) Approximation

As said in Sec. 1, the next step involved is to further reduce each of the transformed and decoupled PDEs given by Eq. (17) (similarly for the other transformed governing differential equations corresponding to (7) and (8)) for j=0,1, . . . , $n-1$ to a set of coupled ODEs using Daubechies scaling function approximation in one of the spatial (*Y)* direction. Similar to time approximation, the transformed variable $\hat{u}_{oj}$ can be discretized at m points in the spatial window [0, L_Y], where L_Y is the length in Y direction. Let $\xi = 0,1,.....,m-1$ be the sampling points, then

$$y = \triangle Y \zeta \qquad (19)$$

where ΔY is the spatial interval between two sampling points. The function $\hat{u}_{oj}(x, y)$ can be approximated by scaling function $\varphi(\xi)$ at an arbitrary scale as

$$\hat{u}_{0j}(x,y) = \hat{u}_{0j}(x,\zeta) = \sum_k \hat{u}_{0lj}(x)\varphi(\zeta - l), \quad l \in \mathbf{Z} \qquad (20)$$

where $\hat{u}_{olj}(x, y)$ (referred as $\hat{u}_{olj}$ hereafter) are the approximation coefficients at a certain spatial dimension x. The other displacements $\hat{v}_{oj}(x, y)$, $\hat{w}_j(x, y)$ can be similarly transformed. Following similar steps as the time approximation, substituting the above approximations in Eq. (17) and taking inner product on both sides with the translates of scaling functions $\varphi(\xi - i)$, where i =*0,1, …….. ,m-1* and using their orthogonal properties, we get m simultaneous ODEs as follows

$$\begin{aligned} A_{11}\frac{d^2\hat{u}_{0ij}}{dx^2} + (A_{12}+A_{66})\frac{1}{\triangle Y}\sum_{l=i-N+2}^{i+N-2}\frac{d\hat{v}_{0lj}}{dx}\Omega_{i-l}^1 \\ + A_{66}\frac{1}{\triangle Y^2}\sum_{l=i-N+2}^{i+N-2}\hat{u}_{0lj}\Omega_{i-l}^2 - B_{11}\frac{d^3\hat{w}_{ij}}{dx^3} - (B_{12}+2B_{66}) \\ \times\frac{1}{\triangle Y^2}\sum_{l=i-N+2}^{i+N-2}\frac{d\hat{w}_{lj}}{dx}\Omega_{i-l}^2 = -I_0\gamma_j^2\hat{u}_{0ij} \quad i = 0,1,\ldots,m-1 \end{aligned} \qquad (21)$$

where N is the order of Daubechies wavelet and Ω_{i-l}^1 and Ω_{i-l}^2 are the connection coefficients for first- and second-order derivative defined in Reference [8]

It can be seen from the ODEs given by Eq. (21), that, similar to time approximation, here also certain coefficients $\hat{u}_{oij}$ near the vicinity of the boundaries (i=0 and i=$m-1$) lie

outside the spatial window [L] defined by i=0,1, . . . ,m−1. These coefficients must be treated properly for finite domain analysis. However, here, unlike time approximation, these coefficients are obtained through periodic extension, but only for free lateral edges, while other boundary conditions may be imposed quite differently using a restraint matrix [9]. The unrestrained, *i.e*., free-free boundary conditions may also be imposed in a similar way using a restraint matrix, but interestingly, it has been seen from the numerical experiments that the use of periodic extension gives accurate results. In addition, it allows decoupling of the ODEs using eigenvalue analysis and thus reduces the computational cost. Here, after expressing the unknown coefficients lying outside the finite domain in terms of the inner coefficients considering periodic extension, the ODEs given by Eq. (21) can be written as a matrix equation of the form

$$A_{11}\left\{\frac{d^2\hat{u}_{0ij}}{dx^2}\right\}+(A_{12}+A_{66})[\Lambda^1]\left\{\frac{d\hat{v}_{0ij}}{dx}\right\}+A_{66}[\Lambda^1]^2\{\hat{u}_{0lj}\}$$
$$=-B_{11}\left\{\frac{d^3\hat{w}_{ij}}{dx^3}\right\}-(B_{12}+2B_{66})[\Lambda^1]^2\left\{\frac{d\hat{w}_{lj}}{dx}\right\}-I_0\gamma_j^2\{\hat{u}_{0ij}\} \tag{22}$$

where Λ^1 is the first-order connection coefficient matrix obtained after periodic extension. The coupled ODEs given by Eq.(22) are decoupled using eigenvalue analysis similar to that done in time approximation. It should be mentioned here that matrix Λ^1 obtained after periodic extension has a circulant form and its eigen parameters are known analytically [10]. Let the eigenvalues be ${}_1\beta_i$, then the decoupled ODEs corresponding to Eq. (22) are

$$A_{11}\frac{d^2\tilde{u}_{0ij}}{dx^2}-{}_1\beta_i(A_{12}+A_{66})\frac{d\tilde{v}_{0ij}}{dx}-\beta_i^2A_{66}\tilde{u}_{0ij}-B_{11}\frac{d^3\tilde{w}_{ij}}{dx^3}$$
$$+\beta_i^2(B_{12}+2B_{66})\frac{d\tilde{w}_{ij}}{dx}=-I_0\gamma_j^2\tilde{u}_{0ij}\quad i=0,1,\ldots,m-1 \tag{23}$$

where $\hat{u}_{oj}$ and similarly other transformed displacements are

$$\tilde{u}_{0j}=\Psi^{-1}\hat{u}_{0j} \tag{24}$$

where Ψ is the eigenvector matrix of Λ^1.

Following exactly similar steps, the final transformed and decoupled form of the Eqs. (7) and (8) (following reduction using temporal approximation) are

$$A_{66}\frac{d^2\tilde{v}_{0ij}}{dx^2} - \imath\beta_i(A_{12}+A_{66})\frac{d\tilde{u}_{0ij}}{dx} - \beta_i^2 A_{22}\tilde{v}_{0ij}$$

$$+ \imath\beta_i(B_{12}+2B_{66})\frac{d^2\tilde{w}_{ij}}{dx^2} - \imath\beta_i^3 B_{22}\tilde{w}_{ij} = -I_0\gamma_j^2\tilde{v}_{0ij} \quad (25)$$

$$B_{11}\frac{d^3\tilde{u}_{0ij}}{dx^3} - \beta_i^2(B_{12}+2B_{66})\frac{d\tilde{u}_{0ij}}{dx} - \imath\beta_i(B_{12}+2B_{66})\frac{d^2\tilde{v}_{0ij}}{dx^2}$$

$$+ \imath\beta_i^3 B_{22}\tilde{v}_{0ij} - D_{11}\frac{d^4\tilde{w}_{ij}}{dx^4} + 2\beta_i^2(D_{12}+2D_{66})\frac{d^2\tilde{w}_{ij}}{dx^2} - \beta_i^4 D_{22}\tilde{w}_{ij}$$

$$= -I_0\gamma_j^2\tilde{w}_{ij} + I_2\gamma_j^2\left(\frac{d^2\tilde{w}_{ij}}{dx^2} - \beta_i^2\tilde{w}_{ij}\right) \quad (26)$$

Similarly, the transformed form of the force boundary conditions given by Eqs. (9)–(12) (following reduction using temporal approximation) are

$$A_{11}\frac{d\tilde{u}_{0ij}}{dx} - \imath\beta_i A_{12}\tilde{v}_{0ij} - B_{11}\frac{d^2\tilde{w}_{ij}}{dx^2} + \beta_i^2(B_{12}+2B_{66})\tilde{w}_{ij} = \tilde{N}_{xij} \quad (27)$$

$$A_{66}\left(-\imath\beta_i\tilde{u}_{0ij} + \frac{d\tilde{v}_{0ij}}{dx}\right) + 2\imath\beta_i B_{66}\frac{d\tilde{w}_{ij}}{dx} = \tilde{N}_{yij} \quad (28)$$

$$-B_{11}\frac{d\tilde{u}_{0ij}}{dx} + \imath\beta_i B_{12}\tilde{v}_{0ij} + D_{11}\frac{d^2\tilde{w}_{ij}}{dx^2} - \beta_i^2 D_{12}\tilde{w}_{ij} = \tilde{M}_{yij} \quad (29)$$

$$B_{11}\frac{d^2\tilde{u}_{0ij}}{dx^2} - \imath\beta_i B_{12}\frac{d\tilde{v}_{0ij}}{dx} - D_{11}\frac{d^3\tilde{w}_{ij}}{dx^3} + \beta_i^2 D_{12}\frac{d^2\tilde{w}_{ij}}{dx^2} - I_2\gamma_j^2\frac{d\tilde{w}_{ij}}{dx}$$

$$= \tilde{V}_{ij} \quad i = 0, 1, \ldots, m-1 \quad (30)$$

The final transformed ODEs given by Eqs. (23),(25), and (26) and the boundary conditions Eqs. (28)–(30) are used for 2D WSEM formulation and is similar to the 2D FSFE technique [1].

Similar to the temporal approximation, the spatial sampling rate ΔY is also determined from the order N of the scaling function used for spatial approximation and the spatial distribution of the load.

The four degrees of freedom per node associated with the element formulation are $\tilde{u}_{oij}$, $\tilde{v}_{oij}$, $\tilde{w}_{ij}$ and $\partial^3\tilde{w}_{ij}/\partial x$ as shown in Fig1.

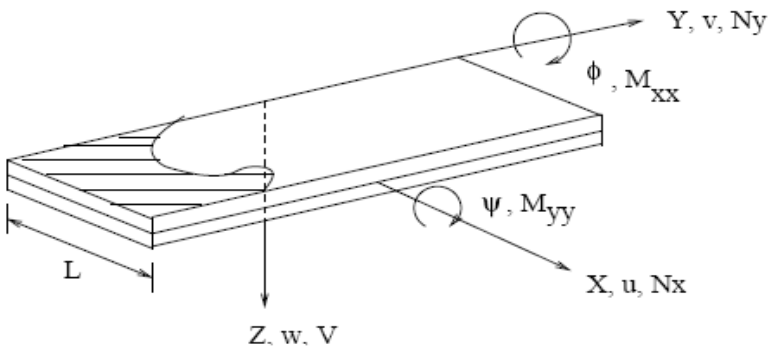

Figure 1: Spectral Plate Element with all the degrees of freedom and Stress Resultants

The corresponding nodal forces are $\tilde{N}_{xij}$, $\tilde{N}_{yij}$, $\tilde{M}_{yij}$ and $\tilde{V}_{ij}$. From the previous sections, for unrestrained lateral edges, we get a set of decoupled ODEs (Eqs. (23), (25), and (26)) for an isotopic plate using CLPT, in a transformed wavelet domain. These equations are required to be solved for $\tilde{u}_{oij}$, $\tilde{v}_{oij}$, $\tilde{w}_{oij}$, and the actual solutions $u_0(x, y, t)$, $v_{0(}x, y, t)$, $w(x, y, t)$ are obtained using inverse wavelet transform twice for spatial Y dimension and time.

It can be seen that the transformed decoupled ODEs have a form that is similar to that in FSEM[1], and thus, the formulation of WSEM from here is similar to FSEM formulation or 1-D WSEM formulation given in Reference [5] . Thus, the formulation is not repeated here. Finally, the transformed nodal forces $\{\tilde{F}^e\}$ and transformed nodal displacements $\{\tilde{u}^e\}$ are related as

$$\{\tilde{\mathbf{F}}^{\mathbf{e}}\} = [\tilde{\mathbf{K}}^e]\{\tilde{\mathbf{u}}^e\} \qquad (31)$$

where $\left[\tilde{K}^e\right]$ is the exact elemental dynamic stiffness matrix. The solution of the Eq. (31) and the assembly of the elemental stiffness matrices to obtain the global stiffness matrix are exactly similar to conventional FE technique.

4. NUMERICAL EXAMPLES.

Here, the axial and transverse wave propagations in composite graphite-epoxy plates of different configurations and ply orientations are studied. The examples used (shown in Figs. 2 (a), (b) and (c)) consist of uniform cantilever plate with symmetric and asymmetric ply lay-ups, cantilever asymmetric plate with ply drop and symmetric folded plate structure. The material properties are as follows, $E1 = 144.48$ GPa, $E2 = E3 = 9.63$ GPa, $G23 = G13 = G12 = 4.128$ GPa, $\nu 23 = 0.3$, $\nu 13 = \nu 12 = 0.02$, $\rho = 1389$ kg/m^3.

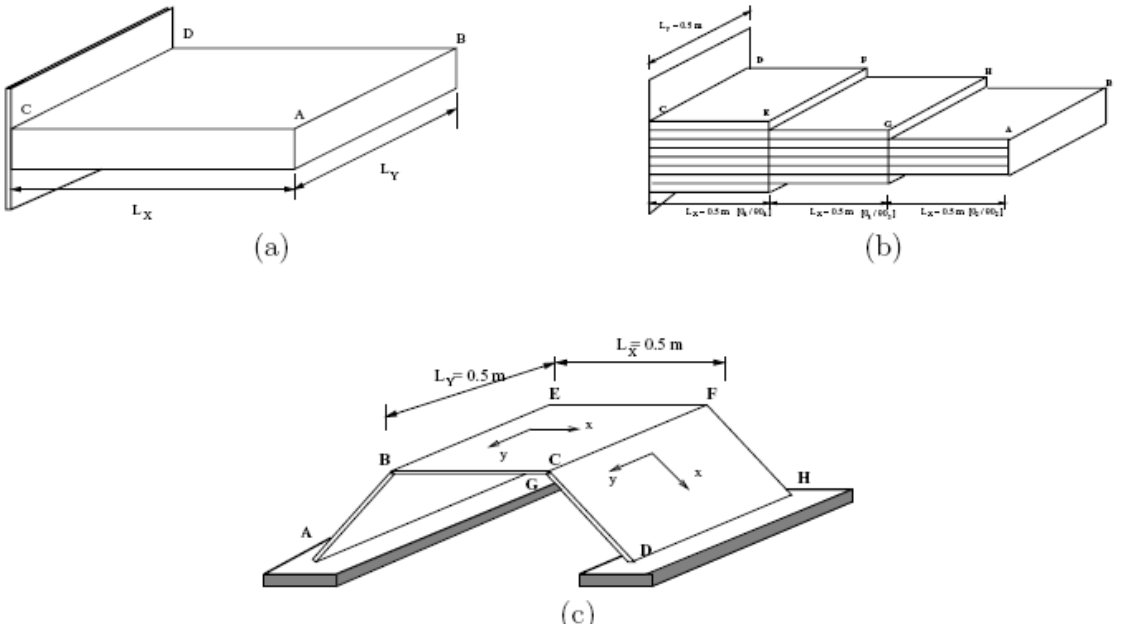

Figure 2: (a) Uniform cantilever, (b) Ply drop and (c) Folded plates.

In all the examples provided, the load applied is an unit impulse and is shown in time and frequency domains in Fig.3. The load is applied at the edge along the Y -axis and has a pulse-like spatial distribution and is given as

$$F(Y) = e^{-(Y/\alpha)^2}$$

where, α is a constant and can be varied to change the Y -axis variation of the load.

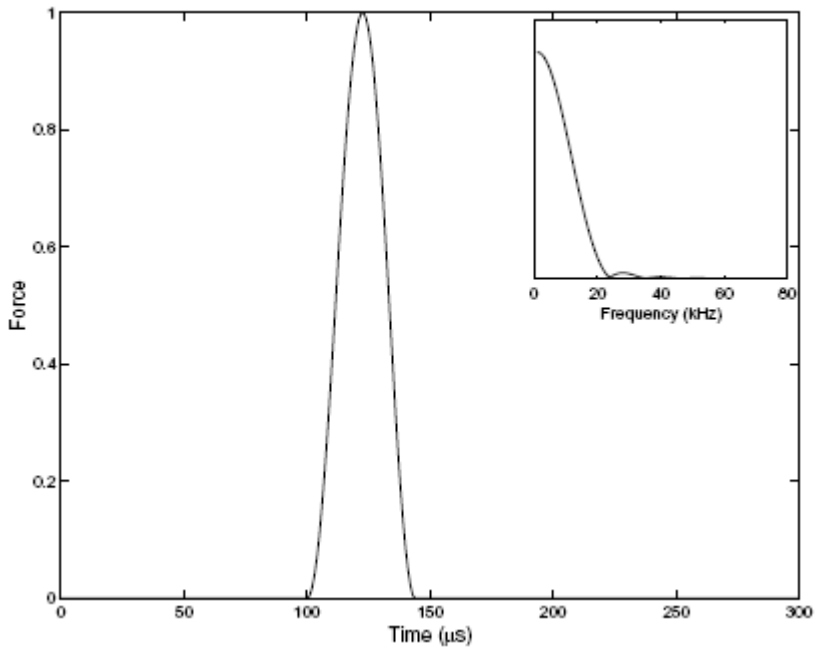

Figure 3: Impact load and Fourier transform of the load (inset)

The 2-D WSEM model is formulated with Daubechies scaling function of order $N = 22$ for temporal approximation and $N = 4$ for spatial approximation. The time sampling rate is $\Delta t = 2\ \mu s$, unless otherwise mentioned, while the spatial sampling rate ΔY is varied depending on LY and load distribution $F(Y)$.

4.1 Uniform Plate

The uniform cantilever plate is shown in Fig. 2(a) and is fixed at one edge CD and free at the other edge AB along Y -axis. Numerical experiments are performed by considering the other two edges AC and BD along X-axis to be free-free. The dimensions are LX and LY along X and Y axes respectively, while the depth (= $2h$) is kept fixed at 0.01 m with 8 laminates. The spectrum relations for the plate with LY = 0.25 m and symmetric ply orientation of [02/904/02] are plotted in Fig. 4 . Figs. 4 (a) and (b) respectively show the real and imaginary parts of the wavenumbers for a Y -wavenumber of 50. It can be seen that the wavenumber has significant real and imaginary parts. This implies that the waves are inhomogeneous in nature, *i.e* they attenuate as they propagate. The wavenumbers have been obtained with $\Delta t = 4\ \mu$s *i.e* for a Nyquist frequency of $fnyq$ = 125 kHz. As said earlier, WSEM predicts accurate wavenumbers only up to a certain fraction pN of Nyquist frequency $fnyq$. This fraction pN for $N = 22$ is approximately 0.6. Thus in Figs. 4.(a) and (b), the wavenumbers are plotted up to a frequency $fN = pNfnyq$ = 75 kHz. In Figs. 5(a) and (b), the real and imaginary parts of the wavenumber of the composite plate with LY = 0.25 m and asymmetric ply lay up of [04/904] are presented respectively. The plots are obtained for a Y wavenumber 50 and time sampling rate $\Delta t = 4\ \mu$s or Nyquist frequency of $fnyq$ = 125 kHz. Even here, the wavenumbers calculated using the present method are correct up to a frequency of $fN = pNfnyq$ = 75 kHz. Similar to plate with symmetric ply lay up, the wavenumbers for asymmetric ply orientation have considerable real and imaginary parts and thus the waves are inhomogeneous in nature. It can be seen that for both symmetric and asymmetric plates, the real part of the wavenumbers show three propagating modes corresponding to axial, lateral and transverse wave propagation. There are three cut-off frequencies which vary with wavenumbers.

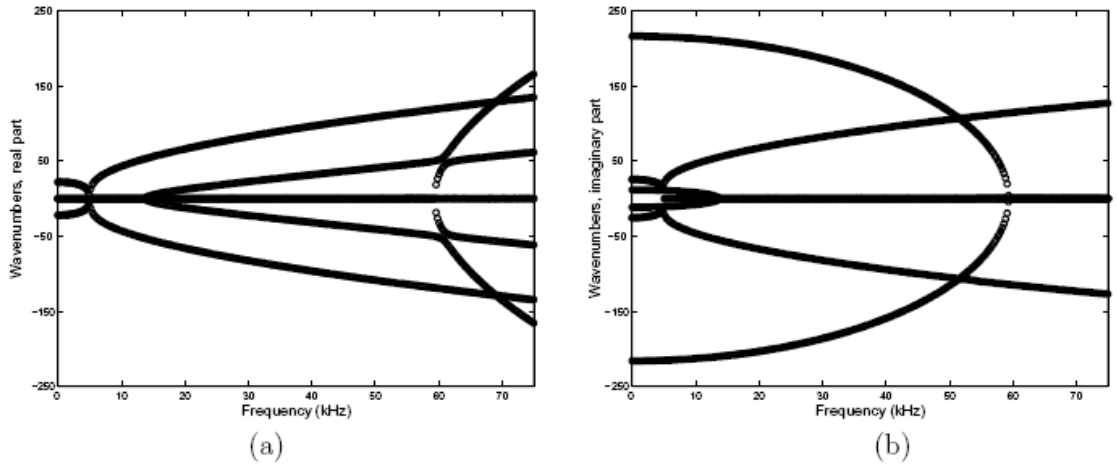

Figure 4: The (a) real and (b) imaginary parts of the wavenumber of plate with symmetric ply lay-up of [02/904/02].

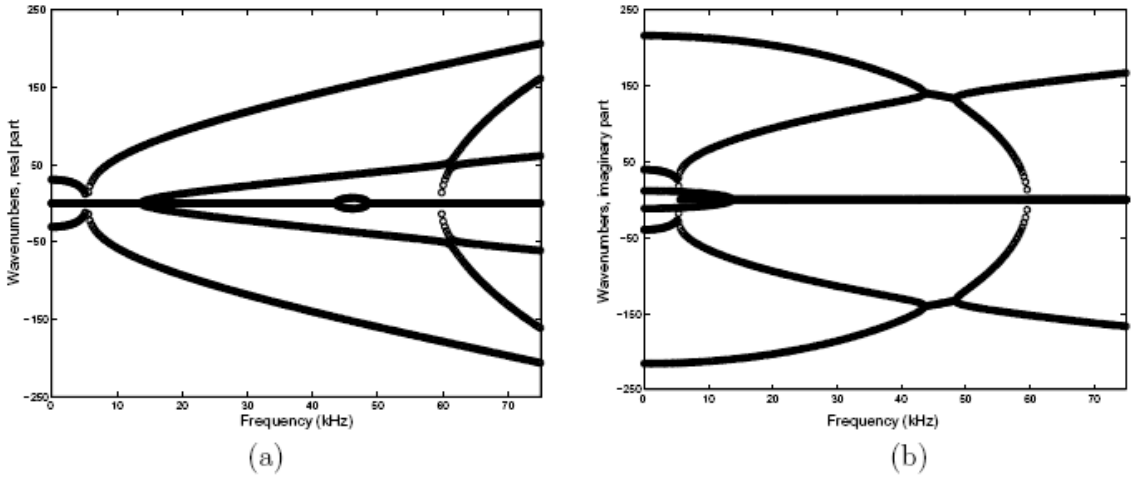

Figure 5: The (a) real and (b) imaginary parts of the wavenumber of plate with asymmetric ply lay-up of [04/904].

Next, the time domain responses of a plate with $LX = 0.5$ m, $LY = 0.25$m and a symmetric ply lay up of [08], simulated using WSFE method are validated with 2-D FE results. In Figs. 6 (a) and (b), respectively, the axial and transverse velocities measured at the mid point of edge AB (see Fig. 2 (a)) of the cantilever plate are plotted and compared with 2-D FE results. The impulse load, shown in Fig. 3, is applied along AB, correspondingly in axial and transverse directions. The Y variation of the load is obtained using $\alpha = 0.03$. As mentioned earlier only one WSEM is used to model the structure and the time window is kept $Tw = 512$ μs with number of sampling points $n = 256$ and $\Delta t = 2$ μs. The number of discretization points along Y -axis is $m = 64$ and thus the spatial sampling rate is $\Delta Y = LY/(m - 1) = 0.004$ m.

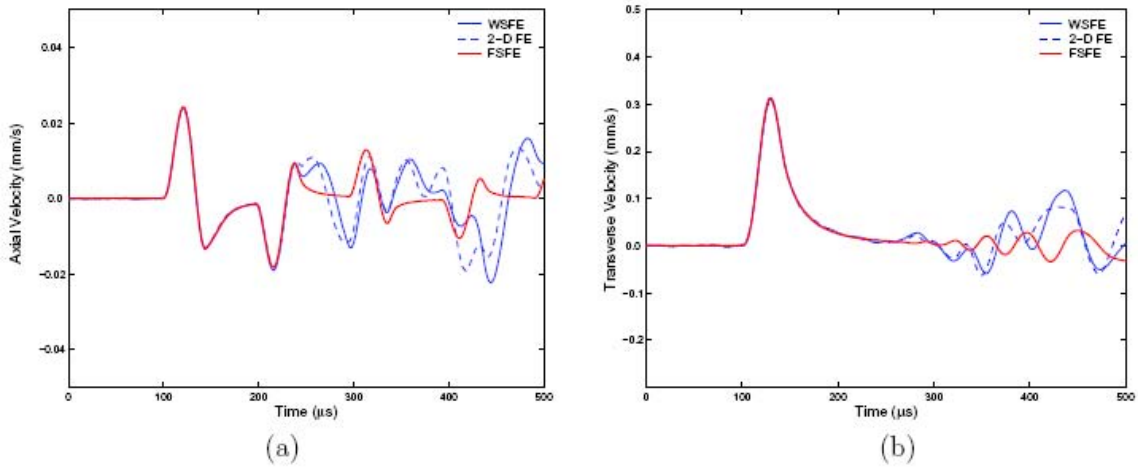

Figure 6: (a) Axial and (b) transverse velocities at mid-point of edge AB in a [0]8 cantilever plate (see Fig. 2(a)) with LX = 0.5 m and LY = 0.25 m due to tip impulse load applied in axial and transverse directions along AB respectively

A very refined mesh with 6432, 4-noded plane stress quadrilateral elements is used for the 2-D FE analysis, while, Newmark's scheme with time step 1 μs was used for time

integration. It can be seen that WSEM and FE results match very well. A comparison is also provided with FSEM results. As stated earlier, it can be seen from the figures, that unlike WSEM, FSEM is unable to accurately capture the reflections from the lateral edges AC and BD in this example. The velocities obtained from FSEM modeling show only the reflections from the fixed edge CD.Thus, for structures with finite or short dimensions, FSEM results will deviate substantially from the actual responses. In addition, simulation with FSFE requires "*throw-off*" element to impart artificial damping to the structure and a large time window Tw = 16384 μs (Δt = 2 μs and n = 8192) to remove the distortions due to "*wrap around*" problem. It should be restated here, that the accuracy of the response simulated using WSEM is independent of the time window Tw which is chosen as required for observation. Similar validation with 2-D FE results are done for the plate with asymmetric ply orientation of [04/904] with the other configurations and loading condition remaining same as the previous example. The parameters for WSEM modeling and the FE mesh are similar to that used in the last example for symmetric lay-up plate. Figs. 7(a) and (b) show the axial and transverse velocities at mid-point of the free edge AB due loading in axial and transverse directions respectively. In this case also the responses obtained with WSFE match well with FE results. In addition, the corresponding velocities simulated using FSEM using the same time window Tw, time Δt and spatial ΔY rates, are also plotted to show the limitations of the FSEM method in modeling finite dimension 2-D structures.

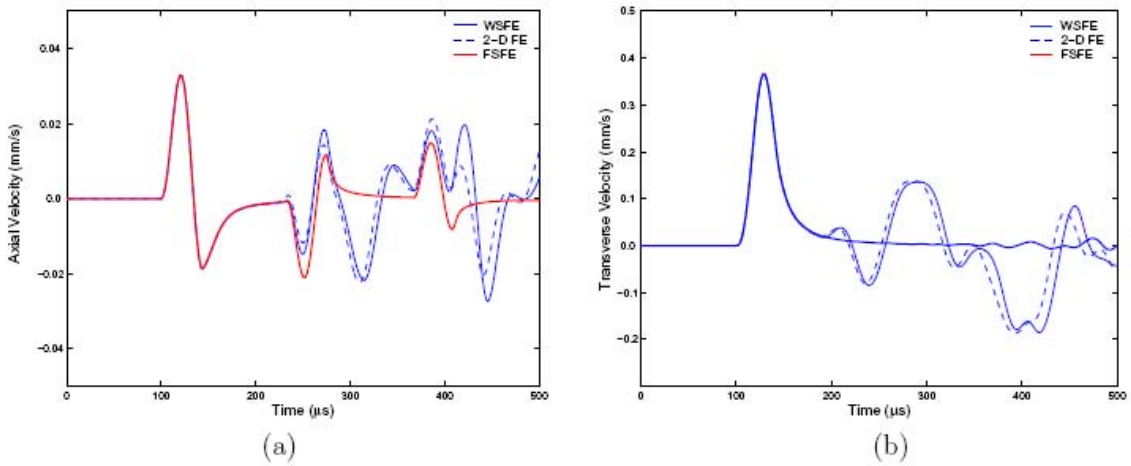

Figure 7: (a) Axial and (b) transverse velocities at mid-point of edge AB in a [04/904] cantilever plate (see Fig. 4.11(a)) with LX = 0.5 m and LY = 0.25 m due to tip impulse load applied in axial and transverse directions along AB respectively.

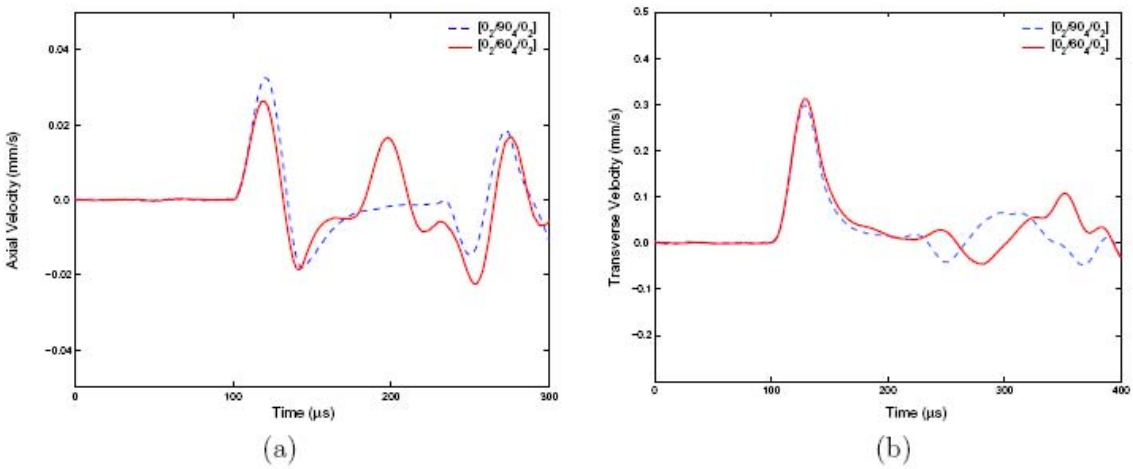

Figure 8: (a) Axial and (b) transverse velocities at mid-point of edge AB in [02/904/02], [02/604/02] and [0]8 cantilever plates (see Fig. 4.11(a)) with LX = 0.5 m and LY = 0.25 m due to tip impulse load applied in axial and transverse directions along AB respectively.

In Fig 8(a), the axial velocities at the mid point of edge AB of cantilever plate shown in Fig. 2(a) are plotted for two different symmetric ply orientations of [02/904/02] and [02/604/02]. The plate has a dimension of LX = 0.5 m and LY = 0.25 m. The impulse loading is similar to that in previous example and is applied in axial direction along edge AB with α = 0.03 for obtaining the Y variation of load. Even here, the simulations are done with a single WSEM, time sampling rate Δt = 2 μs, time window Tw = 512 μs, m = 64 and thus Y sampling rate ΔY = 0.004 m. The corresponding transverse velocities at the mid point of edge AB due transverse loading are plotted in Fig. 8(b). It can be seen that the amplitude of the incident axial waves is more for the ply lay up [02/904/02] than that for [02/604/02]. This is expected as the longitudinal stiffness of the lay up [02/904/02] is more than [02/904/02]. However, the amplitudes do not vary much for the transverse wave velocities. For similar reason the reflections from the lateral edges appear later in [02/904/02] than in [02/604/02]. The axial velocities at the mid point of edge AB of the cantilever plate shown in Fig. 2(a) with asymmetric ply lay-ups [04/904] and [04/604] are plotted in Fig. 9(a).

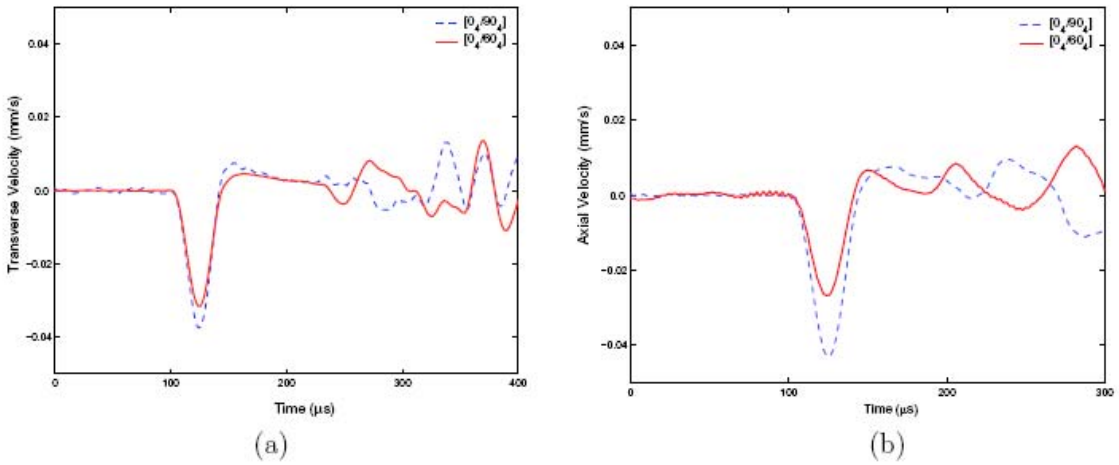

Figure 9: (a) Axial and (b) transverse velocities at mid-point of edge AB in [04/904] and [04/604] cantilever plates (see Fig. 4.11(a)) with LX = 0.5 m and LY = 0.25 m due to tip impulse load applied in transverse and axial directions along AB respectively.

These responses are due to impulse load (see Fig. 3) applied along AB in transverse direction and result from the axial-flexural coupling arising due to the asymmetric ply layup. The Y variation of the load is obtained with $\alpha = 0.03$. The plate dimensions are $LX = 0.5$ m and $LY = 0.25$ m. The parameters involved in WSEM modeling are same as in previous example. Similar to the symmetric configurations, the amplitude of incident wave for [04/904] is more than [04/604] due to reasons as explained before. In Fig. 9(b) the transverse velocities at mid-point of edge AB due to the load applied in axial direction are plotted. These responses also result from the axial-flexural coupling. However, the amplitudes of these velocities arising due to the coupling vary considerably with the ply orientations and as expected are higher for [04/904] due to its lower stiffness.

Figs. 10 (a) and (b) show the snapshots of the axial velocities of the cantilever plate shown in Fig. 2(a) with a symmetric ply orientation of [08], at time instances $T = 250$ μs and $T = 375$ μs respectively. The plate dimensions are $LX = 2.0$ m and $LY = 0.5$ m, and is modeled using single WSEM with $m = 64$ sampling points in Y direction. The impulse load as in Fig. 3 is applied along edge AB in axial direction and the Y variation is obtained with $\alpha = 0.05$. The snapshot at $T = 250$ μs shows the forward moving axial wave, while at $T = 375$ μs the wave reflected from the fixed end of the cantilever plate can be captured. It should be mentioned here that the velocities at all the sampling points along Y direction and at any point along X direction used to obtain the snapshots are obtained from a single simulation. In Figs. 11(a) and (b) the snapshots of the transverse velocities of the cantilever plate shown in Fig. 2(a) with a symmetric ply orientation of [08] are presented for time instances $T = 500$ μs and $T = 1000$ μs respectively. The dimensions and the loading conditions are kept same except that the loading here is applied in transverse direction.

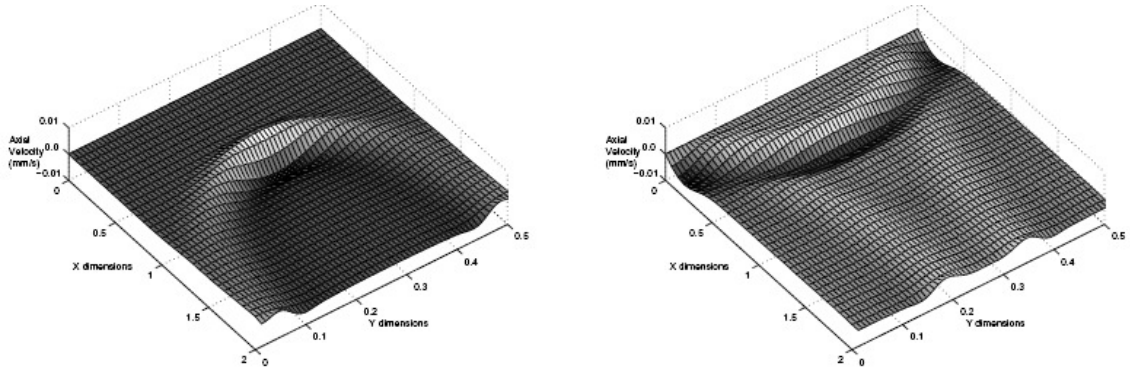

(a) (b)

Figure 10 : Snapshots of axial velocities at time instances (a) T = 250 μs and (b) T = 375 μs in a [0]8 cantilever plate (see Fig. 2(a)) with LX = 2.0 m and LY = 0.5 m due to tip impulse load applied in axial direction.

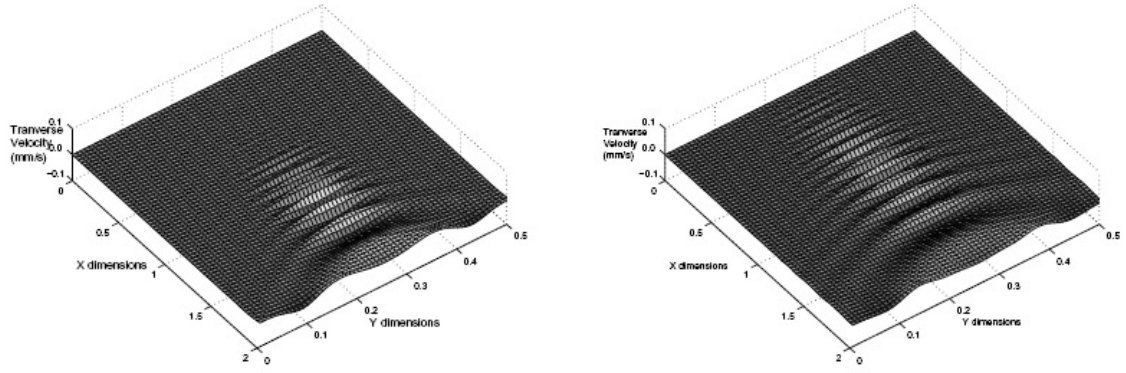

(a) (b)

Figure 11: Snapshots of transverse velocities at time instances (a) T = 500 μs and (b) T = 1000 μs in a [0]8 cantilever plate (see Fig. 2(a)) with LX = 2.0 m and LY = 0.5 m due to tip impulse load applied in transverse direction

WSEM modeling is also performed with the similar parameters. Here, both the snapshots show the forward propagation of the flexural waves and the dispersive nature of these waves can also be observed.

4.2 Ply Dropped and Folded Plates Analysis

Ply dropping is done to taper a composite plate and is in very much use in many composite structures. This example of wave propagation in ply dropped plate due to impulse load is performed to emphasize the effectiveness of the present method in modeling such complex structures. The configuration of the plate is shown in Fig. 2(b) and the overall dimension is LX = 1.5 m in X direction and LY = 0.5 m in Y direction. It is fixed at one end CD and free at the other edge AB. The two lateral edges AC and BD, parallel to Y axis are considered free. The plate is divided into three regions along X direction. From the fixed end to 0.5 m, the ply lay-up is [04/904] and the total thickness is $h1$ = 0.01 m. For the next 0.5 m, two plies are reduced. Here the thickness is $h2$ = 0.0075 m and the lay-up is [03/903]. The last part has a thickness of $h3$ = 0.005 m and the lay-up

is [02/902]. As there are two discontinuities present, three WSEM are assembled to model the plate and the number of sampling points along Y direction is $m = 64$ with $\Delta Y = 0.008$ m. The unit impulse load (see Fig. 3) is applied along edge AB and the Y variation of the load is obtained with $\alpha = 0.05$. In Fig.12 (a), the axial velocity measured at the mid-point of edge AB due to load in axial direction is plotted.

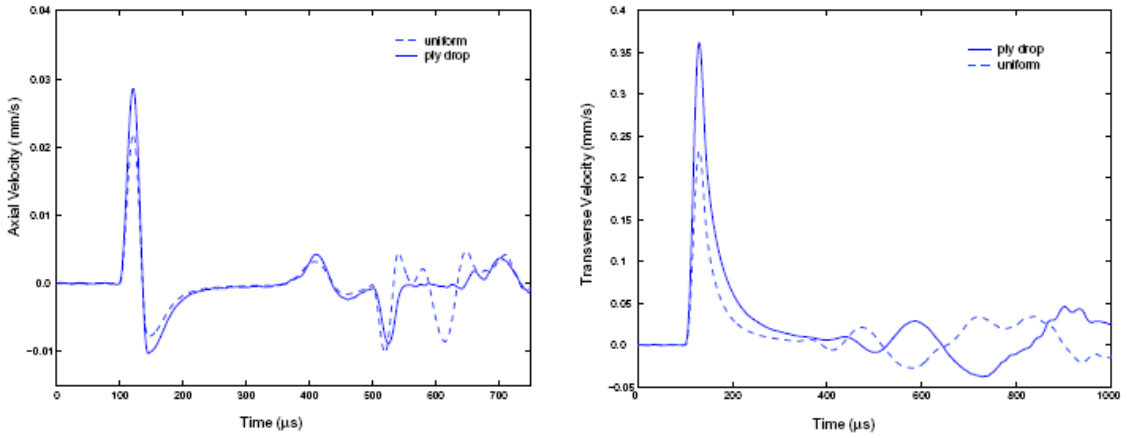

Figure 12: (a) Axial and (b) transverse velocities of asymmetric [04/904] uniform and ply dropped plate (Fig. 2(b) and (c) respectively) with LX = 1.5 m, *LY* = 0.5 m along edgeAB.

The axial velocity of corresponding uniform cantilever plate without ply drop and LX = 1.5 m and LY = 0.5 m, is also plotted for comparison. As expected, the amplitude of the incident wave for the uniform plate is considerably less than that for ply dropped plate. In addition, there are also much differences in the reflected waves arriving later. This is because, apart from the reflections from the lateral free edges and the fixed edge, the response of the ply dropped plate consists of reflections from the discontinuities present. These reflections are absent in the response of the uniform plate In Fig. 12(b), the corresponding transverse velocities due to transverse impulse load, are plotted for both ply dropped and uniform plates. Similar to the axial velocities, here also there is a prominent difference in the amplitudes of the incident waves for the uniform and ply dropped plates. As explained earlier, the reflected waves also show considerable variations.

Next, wave propagation analysis in a folded plate structure, shown in Fig. 2(c), is done using the formulated WSEM method. The folded plate model is obtained by assembling three 2-D WSEM. The number of sampling point along y direction is $m = 32$ for all the three plates. The plates have the same dimensions of Lx =0.5 m and Ly = 0.5 m and a symmetric ply lay-up of [08]. The two slanted plates are at an angle of 60^o to the X direction and the two ends denoted as AG and DH are considered fixed. Assembling is done along the local x direction (see Fig. 2(c)) after the required transformation similar to conventional 1-D FE. The unit impulse load shown in Fig. 3 is applied along edge BE and CF. The Y variation of the load is obtained with $\alpha = 0.1$.

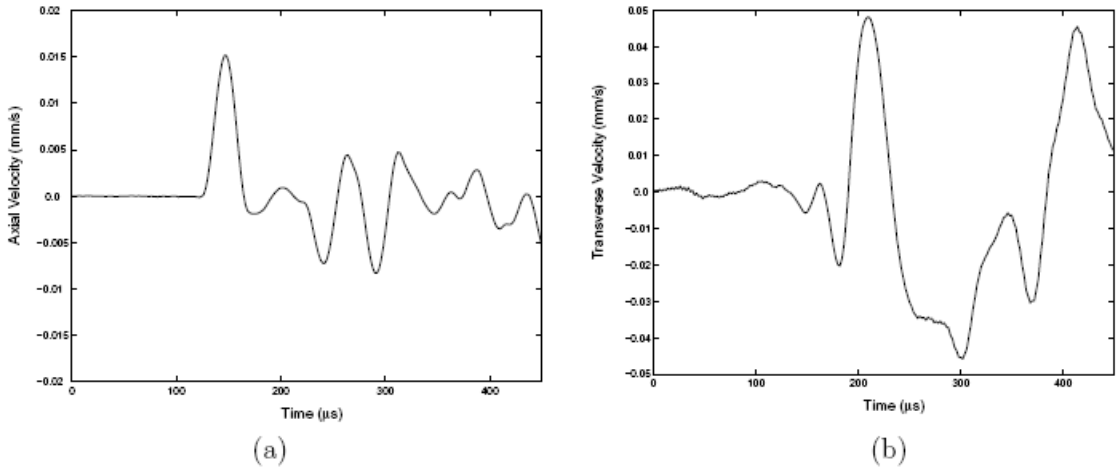

Figure 13: (a) Axial and (b) transverse velocities at mid point of BC of [08] folded plate (Fig. 2(c)) due load applied along edge BE and CF in axial and transverse directions respectively.

In Figs. 13 (a) and (b), the axial and transverse velocities measured at the mid-point of the edge BC, due to the above mentioned load applied in axial (*X*) and transverse (*Z*) directions are plotted respectively.

These numerical experiments show the capability of the present method to analyze the rather complicated folded plate structures. It should be mentioned here that 2-D FSEM cannot be used for modeling such finite dimension structures. In addition even for semi infinite structures, the responses simulated with 2-D FSEM will be highly distorted due to "*wrap around*" as there are multiple reflections from the several discontinuities present

5. CONCLUSIONS

The main aim of this work is to bring out the wave propagation behavior in composite plates. First the wavelet based spectral finite element is developed for composite plate with different ply orientations. The developed WSEM is used to study both frequency and time domain wave characteristics such as the spectrum and dispersion relations. The time domain responses are compared with 2-D FE analysis results and they match well. Comparisons are also provided with the 2-D FSEM analysis results to highlight the efficiency of 2-D WSEM for analysis of finite dimension plates unlike FSEM. Apart from uniform cantilever plate, responses are also simulated for plates with ply-drop and folded structures. These examples show the effectiveness of the proposed methodology in modeling rather complex structures. The next logical extension of this work is to model the damages such as delaminations and fibre breakages in composites. The delamination can be an area delamination or through the depth delamination. First the latter will be attempted in the next year of the project. Similarly, through the width transverse cracks simulating the fiber breakage will also be undertaken in coming year.

ACKNOWLEDGEMENTS

The PI wishes to thank Dr. Kumar V Jata, Programme Manager, Structural Mechanics Programme, AOARD, Tokyo for his sustained support and encouragement throughout this project period. PI also wishes to thank Dr. Ratan Jha, the CO PI of the project from Clarkson University, New York, USA for fruitful discussions during the course of this work. The PI also thanks his former graduate student Dr. Mira Mitra for helping in simulating some of the results in this report.

REFERENCES

1. Gopalakrishnan, S., Chakraborty, A., and Roy Mahapatra, D., *Spectral Finite Element Method,* Springer-Verlag, UK, 2007
2. Doyle, J.F., , *Wave Propagation in Structures,* Springer Verlag, New York, 1997
3. Daubechies, I., *Ten Lectures on Wavelets*, CBMS-NSF Series in Applied Mathematics, SIAM, Philadelphia, 1992.
4. Williams, J. R., and Amaratunga, K., 1997, "A Discrete Wavelet Transform Without Edge Effects Using Wavelet Extrapolation," *J. Fourier Anal. Appl.,* **3**(4), 435–449, 1997.
5. Mitra, M., and Gopalakrishnan, S., "Spectrally Formulated Wavelet Finite Element for Wave Propagation and Impact Force Identification in Connected 1D Waveguides," *Int. J. Solids Struct*., **42**, 4695–4721, 2005.
6. Mitra, M., and Gopalakrishnan, S., "Extraction of Wave Characteristics from Wavelet Based Spectral Finite Element Formulation," *Mech. Syst. Signal Process.*, **20**, 2046–2079, 2006.
7. Reddy, J. N., *Mechanics of Laminated Plates*, CRC Press, Boca Raton, 1997.
8. Beylkin, G., "On the Representation of Operators in Bases of Compactly Supported Wavelets," *SIAM* (*Soc. Ind. Appl. Math.*) *J. Numer. Anal*., **6**(6), 1716–1740., 1992.
9. Chen, M. Q., Hwang, C., and Shih, P., "The Computation of Wavelet-Galerkin Approximation on a Bounded Interval," *Int. J. Numer. Methods Eng*., **39**, pp. 2921–2944, 2006.
10. Davis, P. J., *Interpolation and Approximation*, Blaisdell, New York, 1963.